Blue-Light-Excited Eu³⁺/Sm³⁺ Co-Doped NaLa(MoO₄)₂ Phosphors: Synthesis, Characterizations and Red Emission Enhancement for WLEDs

Man Yan [1], Guanghui Liu [1],*, Jiahao Wen [2] and Yinlong Wang [2],*

[1]   College of Materials Science and Engineering, Nanjing Tech University, Nanjing 210009, China; many230@njtech.edu.cn

[2]   School of Resources, Environment and Materials, Guangxi University, Nanning 530004, China; 18477167778@163.com

*   Correspondence: guanghui@njtech.edu.cn (G.L.); 15507718949@163.com (Y.W.)

Abstract: The system NaLa(MoO₄)₂:Eu³⁺/Sm³⁺ phosphors were prepared by solid-state reaction followed by heat treatment at 450–600 °C. As shown by X-ray powder diffraction, the phosphors had a body-centered tetragonal structure, high phase purity and high crystallinity. The photoluminescence measurements carried out under excitation at 464 nm indicated the main emission at about 615 nm corresponding to the electric dipole transition $^5D_0 \rightarrow {}^7F_2$ of Eu³⁺, which agreed well with the emission wavelengths of the GaN-based blue LED chips. In NaLa(MoO₄)₂:Eu³⁺/Sm³⁺ phosphors, Sm³⁺ can efficiently transfer excitation energy to Eu³⁺, which resulted in a significant improvement of the fluorescence intensity, and the fluorescence intensity of the phosphors calcined at 550 °C maximized at the doping concentrations of Eu³⁺ and Sm³⁺ of 15.0 and 2.0 mol %, respectively. The decay curves and CIE (Commission Internationale de L' Eclairage) coordinates of Sm³⁺ or/and Eu³⁺ doped phosphors were analyzed for the investigation of the energy transfer mechanism and color variation trend. Thus, NaLa(MoO₄)₂:Eu³⁺,Sm³⁺ can be classified as a potential red-emitting phosphor for white light-emitting diodes (WLEDs).

Keywords: luminescence properties; molybdate; red-emitting phosphor; energy transfer

1. Introduction

These days, the white light-emitting diodes (WLEDs) regarded as the new-style solid-state photosources achieve much more research enthusiasm than before owing to the energy conservation and environmental protection, long service time, high reliability and function [1–4]. However, the development of WLEDs is largely limited because there is no excellent red phosphor [5,6]. In the last few years, great attention has been focused on double alkaline rare-earth molybdates in virtue of their unique structures and excellent luminous properties [7–9]. NaLa(MoO₄)₂ pertaining to the double molybdate family is of tetragonal structure with space group I4₁/a wherein Mo⁶⁺ combining with four neighboring O²⁻ forms tetrahedral MoO₄²⁻ anions to make phosphor matrix with high physical–chemical stability [10,11] and both Na⁺ and La³⁺ randomly occupy S₄ lattice sites with no symmetrical center, which is propitious to relieve further parity forbidden of the electric dipole transition of RE³⁺ [12]. Furthermore, the MoO₄²⁻ group can absorb the energy of the ultraviolet light through Mo-O charge transfer interaction, and then improve rare-earth fluorescence materials' luminous efficiency and intensity via transferring energy to rare-earth ions [13,14].

Europium ion (Eu^{3+})-doped compounds are the most promising candidates as the efficient red phosphors for WLEDs due to their advantages of high color purity and the strongest characteristic red light emission peak at about 615 nm attributing to the $^5D_0{\rightarrow}^7F_2$ transition [15–17]. Nowadays, Eu^{3+}-doped molybdates are regarded as excellent red phosphors, but possess low luminescence intensity, improvement of which has been tested through many efforts [18]. For example, Zuo et al. [5] found that red emission intensities of Eu^{3+} were overwhelmingly improved by co-doping Bi^{3+} in the $KLa(MoO_4)_2$ phosphors. Zhou et al. [19] reported that intensity of $LiY(MoO_4)_2:Eu^{3+},Sm^{3+}$ phosphors was heightened when the compounds were prepared by sol–gel process. However, for all we know, no researchers have reported the energy transfer pathway or photoluminescence (PL) properties of the Sm^{3+}/Eu^{3+} co-doped $NaLa(MoO_4)_2$ matrix.

Thus, we synthesized the Eu^{3+} or/and Sm^{3+} doped $NaLa(MoO_4)_2$ phosphors through a solid-state reaction. The influence of a calcination temperature on a crystal phase as well as luminescent intensity being discussed, and the photoluminescence (PL) spectra, decay behaviors and chromatic properties were analyzed at length.

2. Experimental

2.1. Synthesis

The $Eu(NO_3)_3 \cdot 6H_2O$ (99.99%), $Sm(NO_3)_3 \cdot 6H_2O$ (99.9%), $La(NO_3)_3 \cdot 6H_2O$ (99.0%), $NaNO_3$ (99.0%) and $(NH_4)_6Mo_7O_{24} \cdot 4H_2O$ (99.0%) used as raw materials were bought from Shanghai Aladdin Bio-Chem Technology Co., Ltd. (Shanghai, China). The Eu^{3+}-doped $NaLa(MoO_4)_2$ (abbreviated as $NL_{1-x}MO:xEu^{3+}$; the mol % x = 5, 10, 15 and 20%) and Eu^{3+}/Sm^{3+}co-doped $NaLa(MoO_4)_2$ (abbreviated as $NL_{1-x-y}MO:15\%Eu^{3+},ySm^{3+}$; the mol % y = 0, 1, 2, 3, 4 and 5%) phosphors were prepared by solid-state reaction. The stoichiometric mixtures of $NaNO_3$, $La(NO_3)_3 \cdot 6H_2O$, $(NH_4)_6Mo_7O_{24} \cdot 4H_2O$, $Eu(NO_3)_3/Sm(NO_3)_3$ solution (1 M) were ground thoroughly for 1 h in a porcelain mortar to be uniform, and, then, they were oven-dried at 85 °C for 12 h. Finally, appropriate amounts of procedures were calcined in a muffle furnace at 450, 500, 550 or 600 °C for 360 min to form the final products.

2.2. Characterization

The phase composition of the products was determined by the X-ray diffraction (XRD) method (Rigaku-Dmax 2500 X-ray diffractometer (Japanese science and science company, Tokyo, Japan) with graphite monochromatized Cu Kα radiation, scanning rate was 5°/min, 2θ = 10–75°). The photoluminescence excitation (PLE) and photoluminescence (PL) emission spectra were measured on a HORIBA Fluoromax-4 spectrophotometer (HORIBA Ltd, Irvine, CA, America) equipped with a 150 W Xe-lamp, and the fluorescent decay curves were determined by a Hamamatsu Quantaurus–Tau spectrophotometer (Japanese hamamon photonics Ltd, Hamamatsu, Japan) equipped with a 450 W xenon impulse lamp as the excitation source. The entire tests were put into effect under room temperature conditions.

3. Results and Discussion

3.1. XRD

In Figure 1a, the two representative XRD patterns of $NL_{85\%}MO:15\%Eu^{3+}$ and $NL_{83\%}MO:15\%Eu^{3+},2\%Sm^{3+}$ calcined at 550 °C for 6 h are shown. The diffraction peaks were well attributed to pure tetragonal phase $NaLa(MoO_4)_2$ (PDF Card 79-2243, a = b = 0.53424 nm, c = 1.17376 nm), indicating that the doped ions were successfully incorporated into matrix lattice and had not drastically altered the host structure. The presence of foreign phases was not detected. Figure 1b shows the XRD patterns of the products formed at 450, 500, 550 or 600 °C for 6 h. Obviously, the crystalline $NLMO:Eu^{3+}$ has already formed at 450 °C and the sample calcined at 550 °C is better crystallized and possesses stronger and sharper peaks.
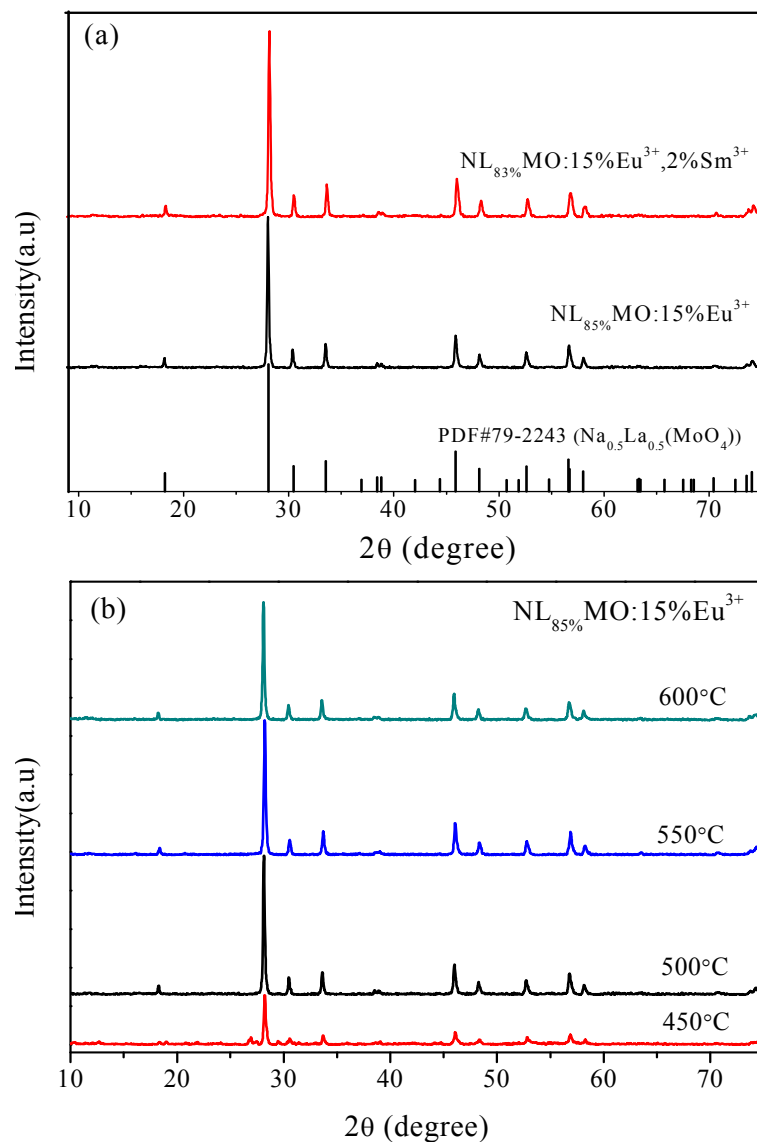
Figure 1. XRD patterns of (**a**) NL$_{83\%}$MO:15%Eu^{3+},2%Sm^{3+} and NL$_{85\%}$MO:15%Eu^{3+} obtained at 550 °C and (**b**) NL$_{85\%}$MO:15%Eu^{3+} formed at different temperatures for 6 h.

3.2. PL Properties of NLMO: Eu^{3+} Phosphors

It is generally known that Eu^{3+} as an excellent activator ion is extensively applied in commercial phosphors because its characteristic emission lines related to the $^5D_0{\rightarrow}^7F_J$ (J = 1–4) transitions are usually distributed in the red spectral region [20]. Clearly, in Figure 2, the PLE spectrum of NL$_{85\%}$MO:15%Eu^{3+} monitored with the emission at 615 nm correspondent to the $^5D_0{\rightarrow}^7F_2$ transition of Eu^{3+} is shown. There is a strong broad band ranging from 220 to 350 nm with a maximum at 265 nm as a result of the O-Mo and O-Eu charge transfers, as well as several sharp peaks within 350–500 nm. It is easy to ascribe the sharp peaks at 382, 394, 416 and 464 nm to the intra-configuration 4f–4f transitions of Eu^{3+} including $^7F_0{\rightarrow}^5G_J$,$^5L_7$, $^7F_0{\rightarrow}^5L_6$, $^7F_0{\rightarrow}^5D_3$ and $^7F_0{\rightarrow}^5D_2$, respectively. Among them, the strongest one at 464 nm is just agreed with the emission wavelengths of the GaN-based blue LED chips. The emission spectrum (PL) obtained under excitation of 464 nm consists of several sharp peaks at 537, 593, 615 and 703 nm due to the transitions of $^5D_1{\rightarrow}^7F_1$ and $^5D_0{\rightarrow}^7F_J$ (J = 1, 2, 4) of Eu^{3+}, respectively. In particular, $^5D_0{\rightarrow}^7F_1$ belongs to magnetic and $^5D_0{\rightarrow}^7F_2$ to electric dipole transitions. According to the Judd–Ofelt theory [21,22], if Eu^{3+} is located at inversion symmetry, the $^5D_0{\rightarrow}^7F_1$ transition, which is scarcely affected by the crystal field environment of Eu^{3+}, will play a leading role

in the PL spectra and the phosphors emit an orange-red light when excited. Otherwise, the $^5D_0 \rightarrow ^7F_2$ transition is stronger and the phosphors emit a red light when excited. Moreover, the $^5D_0 \rightarrow ^7F_2$ transition is dominant in the PL spectra, which clearly indicates that Eu^{3+} occupies the La^{3+} site with anti-inversion symmetry and it means high red color purity. Here, the effects of Eu^{3+} concentration and synthesizing temperature on emission intensity are also shown in Figures 3 and 4. Obviously, the optimal Eu^{3+} concentration and calcination temperature are 15 mol % and 550 °C, respectively, which were selected as the optimal conditions in the following experiments.
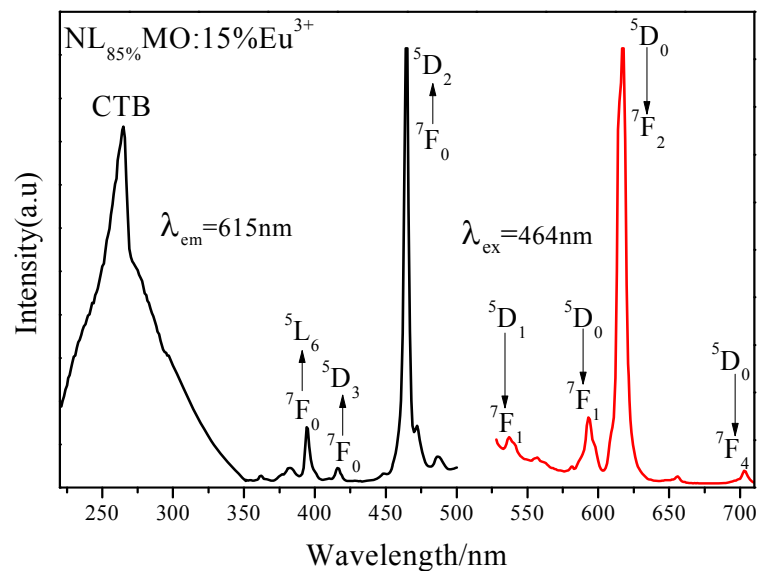

Figure 2. Excitation (λ_{em} = 615 nm) and emission (λ_{ex} = 464 nm) spectra of $NL_{85\%}MO:15\%Eu^{3+}$.

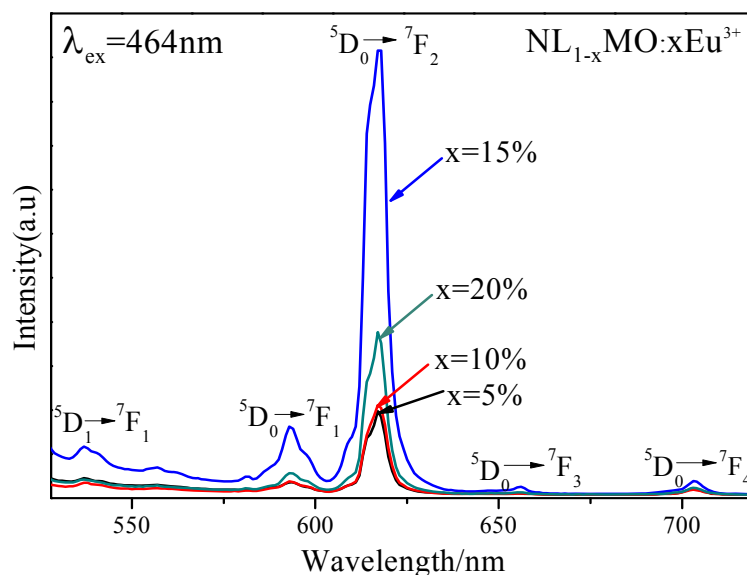**Figure 3.** Emission (λ_{ex} = 464 nm) spectra of $NaLa(MoO_4)_2$ with Eu^{3+} concentration at 5, 10, 15 and 20 mol %.

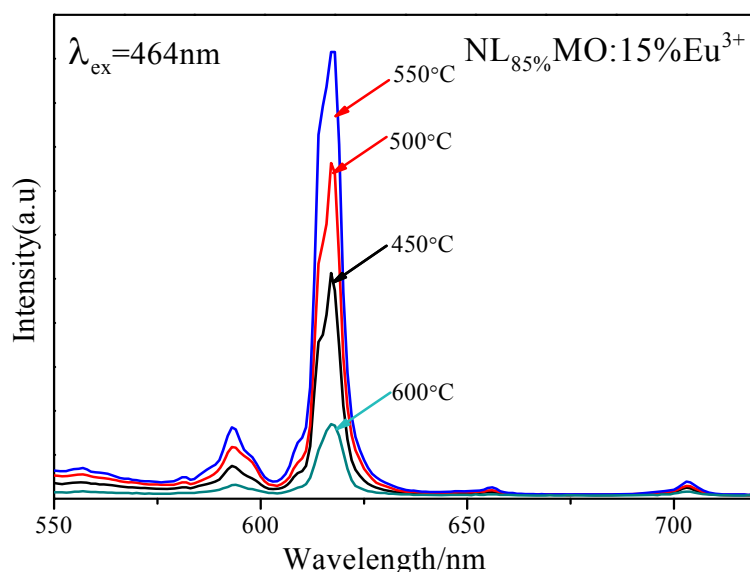**Figure 4.** Emission (λ_{ex} = 464 nm) spectra of $NL_{85\%}MO:15\%Eu^{3+}$ obtained at different calcination temperatures.

3.3. PL Properties and Energy Transfer Pathway of NLMO:Eu³⁺/Sm³⁺ Phosphors

To investigate how Sm^{3+} transfers its energy to Eu^{3+} in NLMO, we analyzed the PLE and PL spectra in detail. Differing from the PLE spectrum of $NL_{85\%}MO:15\%Eu^{3+}$, that of $NL_{83\%}MO:15\%Eu^{3+},2\%Sm^{3+}$ consists of the characteristic excitation peaks of Eu^{3+} at about 395, 464 and 535 nm and an excitation peak at about 403 nm attributed to the transition of $^6H_{5/2}\rightarrow^4F_{7/2}$ of Sm^{3+} (Figure 5).

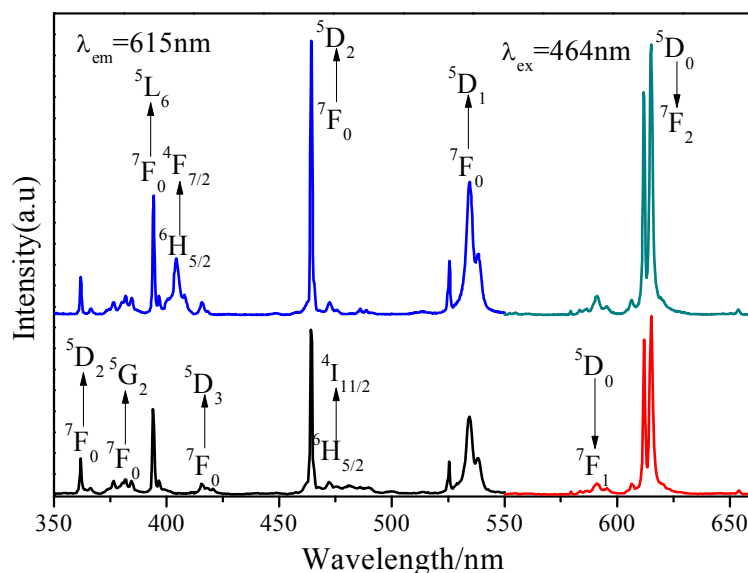**Figure 5.** PLE and PL spectra of $NL_{85\%}MO:15\%Eu^{3+}$ and $NL_{83\%}MO:15\%Eu^{3+},2\%Sm^{3+}$.

The PL spectrum of $NL_{83\%}MO:15\%Eu^{3+},2\%Sm^{3+}$ excited at 403 nm is closely similar to those excited at 393 and 465 nm, while the emission bands at 537 nm correspondent to the $^5D_1\rightarrow^7F_1$ transition of Eu^{3+} and the relative peak intensities are different (Figure 6). The three PL spectra exhibit two significant emission peaks at about 593 and 615 nm related to the transitions of $^5D_0\rightarrow^7F_1$ and $^5D_0\rightarrow^7F_2$ of Eu^{3+}, respectively, indicating the Sm^{3+} transferred efficiently its excitation energy to

Eu^{3+}. Further comparison shows that there are the emission bands at 537 nm in $NLMO:Eu^{3+}$ and $NLMO:Eu^{3+}/Sm^{3+}$ excited at 393 and 464 nm, but not in $NLMO:Eu^{3+}/Sm^{3+}$ when excited at 405 nm, while there are still other transitions of Eu^{3+}. Therefore, the energy transfer just occurs from the $^4G_{5/2}$ state of Sm^{3+} to the $^5D_0$ state rather than the $^5D_1$ state of Eu^{3+}. The probable energy transfer pathway, as determined from the analysis above, is displayed in Figure 7. The electrons of Sm^{3+}, after being excited into $^4K_{11/2}$ level, rapidly relaxed down to the $^4G_{5/2}$ state owing to lattice vibration, and then returned to the ground states through the energy transfer to the $^5D_0$ level rather than the $^5D_1$ level of Eu^{3+} [23,24].
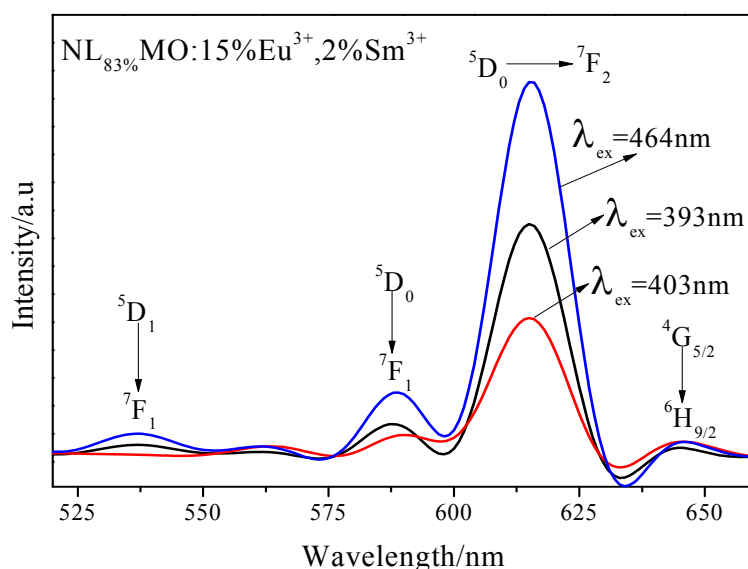

Figure 6. PL spectra of $NL_{83\%}MO:15\%Eu^{3+},2\%Sm^{3+}$ under the excitation at 393,403 and 465 nm.

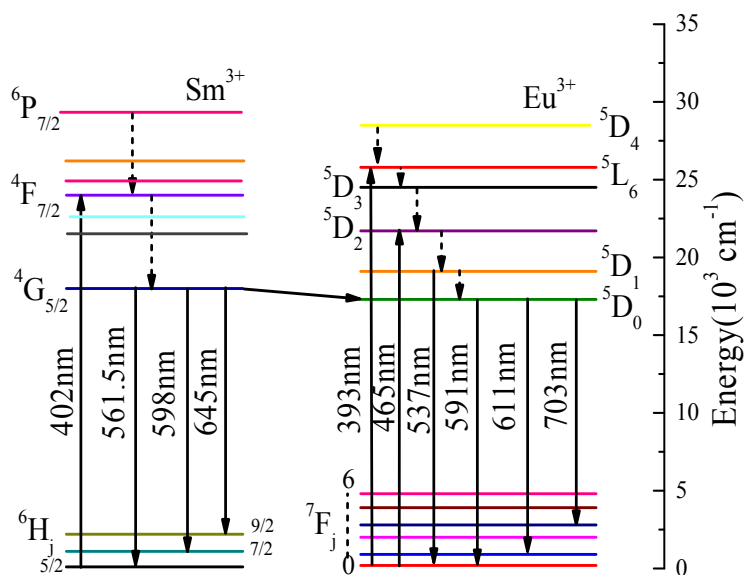**Figure 7.** The energy transfer pathway between Eu^{3+} and Sm^{3+} in $NaLa(MoO_4)_2$.

Figure 8a,b exhibits the PLE (λ_{em} = 615 nm) and PL(λ_{ex} = 464 nm) spectra of $NL_{85\%-y}MO:15\%Eu^{3+},ySm^{3+}$ (y = 0, 1, 2, 3, 4 and 5%), respectively. Clearly, with y increasing from 0 to 2%, the characteristic excitation and emission intensities of Eu^{3+} are enhanced because Sm^{3+} transfer its energy to Eu^{3+}, and, then, the intensities are weakened because of concentration quenching. Moreover,

the fluorescence intensity of $NL_{83\%}MO:15\%Eu^{3+},2\%Sm^{3+}$ is 1.47 times that of $NL_{83\%}MO:15\%Eu^{3+}$. The results further demonstrate the efficient energy transfer from Sm^{3+} to Eu^{3+}.
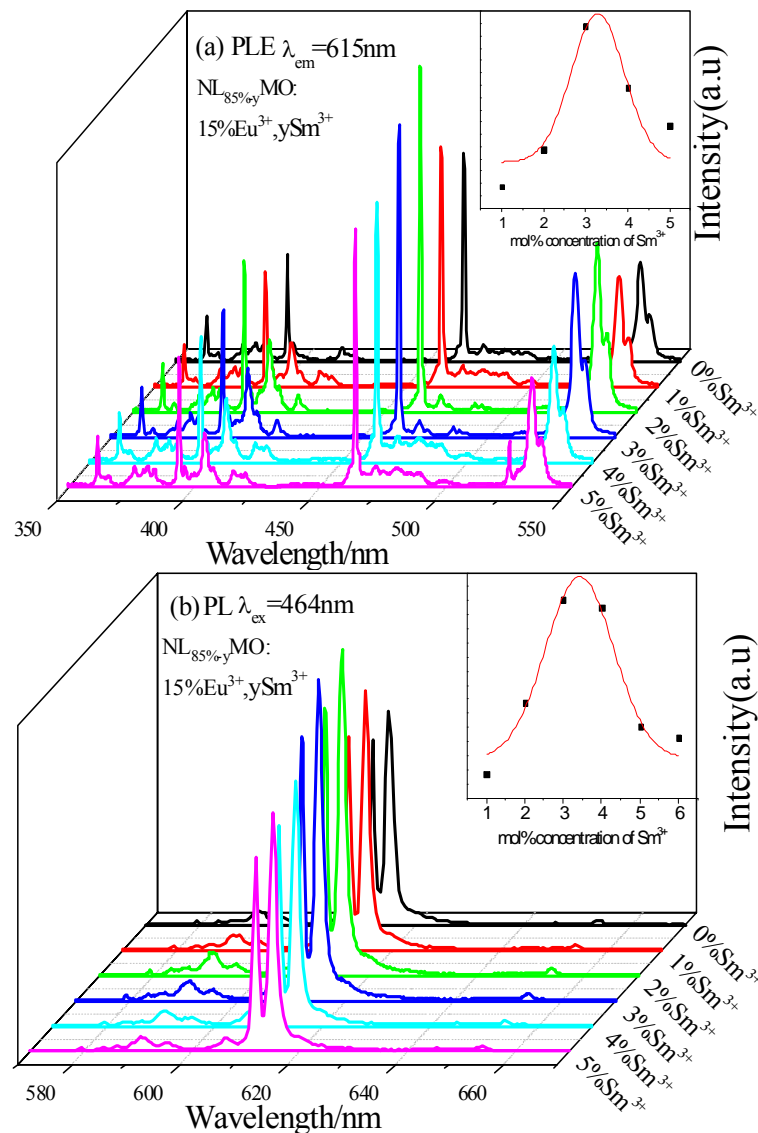

Figure 8. (**a**,**b**) excitation spectra (λ_{em} = 615 nm) and emission spectra (λ_{ex} = 464 nm) of $NL_{85\%-y}MO:15\%Eu^{3+},ySm^{3+}$ (y = 0, 1, 2, 3, 4 and 5%).

3.4. Decay Curves and Energy Transfer Mechanism of NLMO:Eu³⁺/Sm³⁺ Phosphors

To deeply explore the interaction mechanism of energy transfer from Sm^{3+} to Eu^{3+} in the NLMO matrix, we measured the fluorescence lifetime of $NL_{98\%-x}MO:xEu^{3+},2\%Sm^{3+}$ (x = 0, 5, 10, 15 and 20%). The test results and decay curves were shown in Table 1 and Figure 9, respectively.

The fluorescence lifetime of Sm^{3+} is gradually shortened along with the concentration of Eu^{3+} increased from 0 to 20%, which is due to the fact that the energy transfer between Sm^{3+} and Eu^{3+} shortens the time for excited-electrons to move back to the ground state. To more intuitively understand the energy transfer from Sm^{3+} to Eu^{3+}, the efficiency (η_{ET}) of energy transfer from Sm^{3+} to Eu^{3+} was calculated using the following formula [24,25] and the results are also listed in Table 1:

$$\eta_{ET} = 1 - \frac{\tau_s}{\tau_{s0}}, \tag{1}$$

where τ_{s0} and τ_s are the lifetime durations of the donor (Sm^{3+}) without and with the acceptor (Eu^{3+}), respectively. All of the above results strongly confirm that Sm^{3+} transfers its excitation energy to Eu^{3+} in the NaLa $(MoO_4)_2$ matrix.
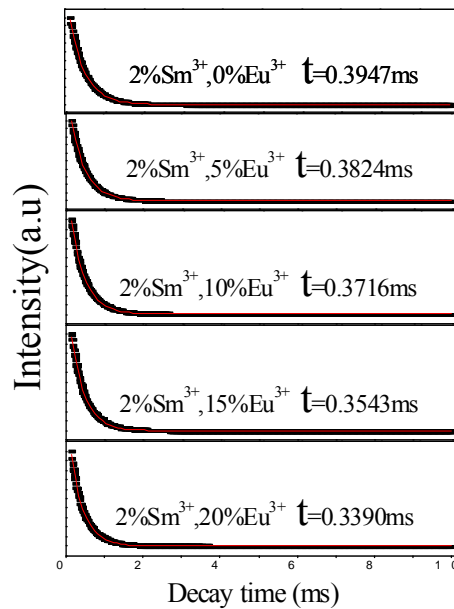

Figure 9. PL decay curves of $NL_{98\%-x}MO:xEu^{3+},2\%Sm^{3+}$.

Table 1. Energy transfer efficiency, distance, lifetime of $NL_{98\%-x}MO:xEu^{3+},2\%Sm^{3+}$.

Xc/mol %	η_{ET}/%	R_{Sm-Eu}/nm	τ_s/ms
2	-	2.5196	0.3947
7	3.116	1.6595	0.3824
12	5.853	1.3866	0.3716
17	10.236	1.2346	0.3543
22	14.112	1.1329	0.3390

Energy is transferred through primarily exchange interaction and multipolar interaction, when the distance, R, between the donor ion and the acceptor ion is less than 0.5 nm and more than 0.5 nm, respectively [26,27]. R_{Sm-Eu} between Eu^{3+} and Sm^{3+} in the NaLa$(MoO_4)_2$ matrix can be calculated as follows [28] (Table 1):

$$R_{Sm-Eu} = 2\left(\frac{3V}{4\pi\chi_C N}\right)^{1/3}, \tag{2}$$

where V is the unit cell volume, χ_c is the total doping mol % concentration of Sm^{3+} and Eu^{3+}, and N is the number of cation sites. For the NaLa$(MoO_4)_2$ crystals, V = 0.33501 nm^3 and N = 2. Based on the above data, the R_{Sm-Eu} of $NL_{98\%-x}MO:xEu^{3+},2\%Sm^{3+}$ (x = 0%, 5%, 10%, 15% and 20%) can be calculated (Table 1). Obviously, the R_{Sm-Eu} values are much greater than 0.5 nm, indicating the exchange interaction is greatly limited. Therefore, Sm^{3+} transfers its energy to Eu^{3+} through the multi-pole interaction mechanism. According to the Dexter formula [29] and Reisfeld approximation method [30] of the electric multi-pole interaction mechanism, the following relation can be obtained:

$$\frac{\tau_s}{\tau_{s0}} \propto C^{\alpha/3}, \tag{3}$$

where C is the doping mol % concentration of Sm^{3+} and Eu^{3+}, and α is relationship index. The values of α correspondent to dipole–dipole, dipole–quadrupole and quadrupole–quadrupole interactions are

6, 8 and 10, respectively. Figure 10a–c shows the Gauss plot of the linear dependency between τ_{s0}/τ_s and $C^{\alpha/3}$. Clearly, R^2, the goodness of fit, is closer to 1 at $\alpha = 10$, meaning Sm^{3+} transfers its energy to Eu^{3+} in the $NaLa(MoO_4)_2$ matrix by the mechanism of quadrupole–quadrupole interaction.

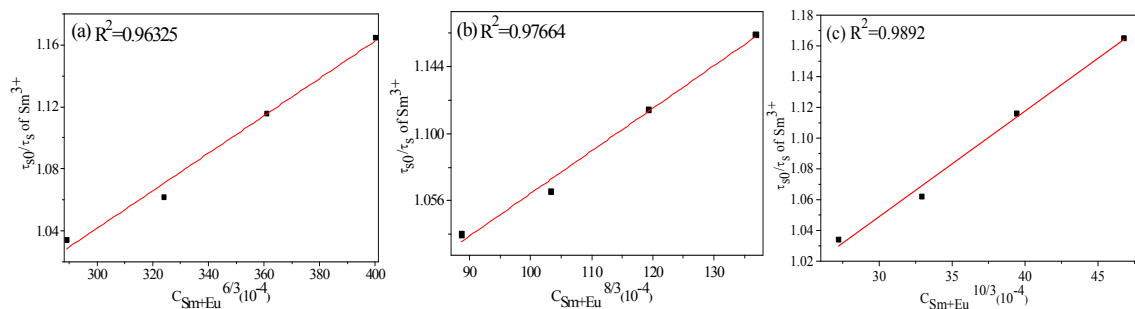**Figure 10.** Dependence of τ_{s0}/τ_s on $C^{\alpha/3}$ with $\alpha = $ (**a**) 6, (**b**) 8, (**c**) 10.

3.5. Chromaticity Coordinate Analysis

To investigate the luminous color of the phosphors, we depicted the CIE chromaticity diagrams of $NL_{85\%-y}MO:15\%Eu^{3+},ySm^{3+}$ when they are excited at 464 nm (Figure 11). The CIE coordinates are listed in Table 2. As seen, the emission light can be regularly shifted from orange to red with the Sm^{3+} molar ratio increasing with a maximum at (0.65, 0.35), which is very close to the CIE chromaticity coordinates (0.67, 0.33) of the standard red light, indicating $NLMO:Eu^{3+},Sm^{3+}$ has a potential application prospect in blue-light-excited WLEDs.

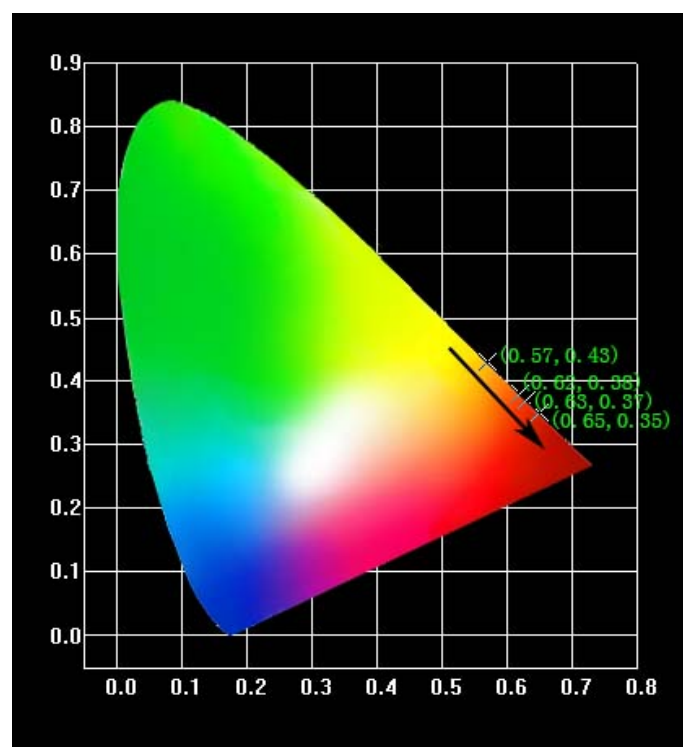**Figure 11.** CIE chromaticity diagram of $NL_{85\%-y}MO:15\%Eu^{3+},ySm^{3+}$ phosphors excited at 464 nm.

Table 2. CIE chromaticity coordinates (x, y) of $NL_{85\%-y}MO:15\%Eu^{3+},ySm^{3+}$ (y = 0, 1, 2, 3, 4 and 5%) excited at 464 nm.

$NL_{85\%-y}MO:15\%Eu^{3+},ySm^{3+}$/%	CIE x	CIE y
y = 0	0.57	0.43
1	0.62	0.38
2	0.63	0.37
3	0.65	0.35
4	0.65	0.35
5	0.65	0.35

4. Conclusions

We prepared the $NLMO:Eu^{3+}/Sm^{3+}$ phosphors via solid-station reaction at 450–600 °C and analyzed their fluorescence spectra. The X-ray diffraction analysis showed that the phosphors possess a body-centered tetragonal structure with high purity and crystallinity. The fluorescence spectrum observation indicates that the phosphor has the strongest excitation and emission peaks at 464 and 615 nm, respectively. The composition possesses a potential for WLEDs because of efficiently emitting red when excited by blue light. In-depth analysis of fluorescence spectra, fluorescence lifetime and inter-ion distance reveals that the energy transfer from the $^4G_{5/2}$ state of Sm^{3+} to the $^5D_0$ state of Eu^{3+} is achieved via the quadrupole–quadrupole mechanism, and it finally broadened the absorption band of Eu^{3+} and enhanced the luminous intensity.

Author Contributions: G.L. and M.Y. conceived and designed the experiments; Y.W. and J.W. performed the experiments and analyzed the data; Y.W. contributed reagents/materials/analysis tools; G.L. and M.Y. wrote the paper.

Conflicts of Interest: The authors declare no conflict of interest.

References

1. Liu, W.R.; Huang, C.H.; Yeh, C.W.; Chiu, Y.C.; Yeh, Y.T.; Liu, R.S. Single-phased white-light-emitting $KCaGd(PO_4)_2:Eu^{2+},Tb^{3+},Mn^{2+}$ phosphors for LED applications. *RSC Adv.* **2013**, *3*, 9023–9028. [CrossRef]
2. Hou, D.; Liang, H.; Xie, M.; Ding, X.; Zhong, J.; Su, Q.; Tao, Y.; Huang, Y.; Gao, Z. Bright green-emitting, energy transfer and quantum cutting of $Ba_3Ln(PO_4)_3:Tb^{3+}$(Ln = La, Gd) under VUV-UV excitation. *Opt. Express* **2011**, *19*, 11071. [CrossRef] [PubMed]
3. Long, J.; Luo, Z.; Wang, T.; Pan, L.; Long, Q.; Liao, S.; Huang, Y.; Zhang, H. Enhanced photoluminescence and energy transfer in the novel red emitting phosphors $SrZn_2(PO_4)_2:Eu^{3+},Tb^{3+},Li^+$. *J. Mater. Sci. Mater. Electron.* **2017**, *28*, 1–4. [CrossRef]
4. Chen, Y.; Wang, J.; Liu, C.; Kuang, X. A host sensitized reddish-orange $Gd_2MoO_6:Sm^{3+}$ phosphor for light emitting diodes. *Appl. Phys. Lett.* **2011**, *98*, 191101. [CrossRef]
5. Zuo, H.; Liu, Y.; Li, J.; Shi, X.; Ma, S.; Zhao, M. Enhancement of red emission in $KLa(MoO_4)_2:Eu^{3+},Bi^{3+}$ phosphor for WLEDs. *Ceram. Int.* **2015**, *41*, 14834–14838. [CrossRef]
6. Jiao, M.; Lv, W.Z.; Lu, W.; Zhao, Q.; Shao, B.Q.; You, H.P. Optical properties and energy transfer of a novel $KSrSc_2(PO_4)_3:Ce^{3+}/Eu^{2+}/Tb^{3+}$ phosphor for white light emitting diodes. *Dalton Trans.* **2015**, *44*, 4080–4087. [CrossRef] [PubMed]
7. Atuchin, V.V.; Chimitova, O.D.; Gavrilova, T.A. Synthesis, structural and vibrational properties of microcrystalline $RbNd(MoO_4)_2$. *J. Cryst. Growth* **2011**, *318*, 683–686. [CrossRef]
8. Atuchin, V.V.; Chimitova, O.D.; Adichtchev, S.V. Synthesis, structural and vibrational properties of microcrystalline β-$RbSm(MoO_4)_2$. *Mater. Lett.* **2013**, *106*, 26–29. [CrossRef]
9. Chang, S.L.; Aleksandrovsky, A.S.; Molokeev, M.S. Microwave synthesis and spectroscopic properties of ternary scheelite-type molybdate phosphors $NaSrLa(MoO_4)_3:Er^{3+}, Yb^{3+}$. *J. Alloy. Compd.* **2017**, *713*, 156–163.

10. Wang, Y.; Lin, C.; Zheng, H.; Sun, D.; Li, L.; Chen, B. Fluorescent and chromatic properties of visible-emitting phosphor $KLa(MoO_4)_2:Sm^{3+}$. *J. Alloy. Compd.* **2013**, *559*, 123–128. [CrossRef]

11. Du, P.; Yu, J.S. Energy transfer mechanism and color controllable luminescence in Dy^{3+}/Eu^{3+}-codoped $NaLa(MoO_4)_2$ phosphors. *J. Alloy. Compd.* **2015**, *653*, 468–473. [CrossRef]

12. Li, G.; Lan, S.; Li, L.; Li, M.; Bao, W.; Zou, H.; Xu, X.; Gan, S. Tunable luminescence properties of $NaLa(MoO_4)_2:Ce^{3+},Tb^{3+}$ phosphors for near UV-excited white light-emitting-diodes. *J. Alloy. Compd.* **2012**, *513*, 145–149. [CrossRef]

13. Wu, H.; Chen, H.; Liu, Y.; Lu, Y.; Zhang, D. Highly uniform $NaLa(MoO_4)_2:Eu^{3+}$ microspheres: Microwave-assisted hydrothermal synthesis, growth mechanism and enhanced luminescent properties. *J. Mater. Sci. Mater. Electron.* **2014**, *25*, 3109–3115. [CrossRef]

14. Kumar, A.; Kumar, J. Perspective on europium activated fine-grained metal molybdate phosphors for solid state illumination. *J. Mater. Chem.* **2011**, *21*, 3788. [CrossRef]

15. Atuchin, V.V.; Aleksandrovsky, A.S.; Chimitova, O.D. Synthesis and spectroscopic properties of monoclinic α-$Eu_2(MoO_4)_3$. *J. Phys. Chem. C* **2014**, *28*, 15404–15411. [CrossRef]

16. Shi, P.; Xia, Z.; Molokeev, M.S. Crystal chemistry and luminescence properties of red-emitting $CsGd_{1-x}Eu_x(MoO_4)_2$ solid-solution phosphors. *Dalton Trans.* **2014**, *25*, 9669–9676. [CrossRef] [PubMed]

17. Atuchin, V.V.; Subanakov, A.K.; Aleksandrovsky, A.S. Structural and spectroscopic properties of new noncentrosymmetric self-activated borate $Rb_3EuB_6O_{12}$ with B_5O_{10} units. *Mater. Des.* **2018**, *140*, 488–494. [CrossRef]

18. Neeraj, S.; Kijima, N.; Cheetham, A.K. Novel red phosphors for solid-state lighting: The system $NaM(WO_4)_{2-x}(MoO_4)_x:Eu^{3+}$ (M = Gd,Y,Bi). *Chem. Phys. Lett.* **2004**, *387*, 2–6. [CrossRef]

19. Zhou, X.; Wang, G.; Zhou, T.; Zhou, K.; Li, Q.; Wang, Z. Luminescence enhancement in Eu^{3+}, Sm^{3+} co-doped $LiY(MoO_4)_2$ nano-phosphors by sol-gel process. *J. Nanosci. Nanotechnol.* **2014**, *14*, 3494. [CrossRef] [PubMed]

20. Du, P.; Bharat, L.K.; Yu, J.S. Strong red emission in Eu^{3+}/Bi^{3+} ions codoped $CaWO_4$ phosphors for white light-emitting diode and field-emission display applications. *J. Alloy. Compd.* **2015**, *633*, 37–41. [CrossRef]

21. Judd, B.R. Optical absorption intensities of rare-earth ions. *Phys. Rev.* **1962**, *127*, 750–761. [CrossRef]

22. Ofelt, G.S. Intensities of Crystal Spectra of Rare-Earth Ions. *J. Chem. Phys.* **1962**, *37*, 511–520. [CrossRef]

23. Bi, W.; Meng, Q.; Sun, W. Luminescent properties and energy transfer mechanism of $NaGd(MoO_4)_2:Sm^{3+}$, Eu^{3+} phosphors. *Ceram. Int.* **2016**, *42*, 14086–14093. [CrossRef]

24. Jin, Y.; Hao, Z.D.; Zhang, X.; Luo, Y.S.; Wang, X.J.; Zhang, J.H. Dynamical processes of energy transfer in red emitting phosphor $CaMo(W)O_4:Sm^{3+},Eu^{3+}$. *Opt. Mater.* **2011**, *33*, 1591–1594. [CrossRef]

25. Rai, S.; Hazarika, S. Fluorescence dynamics of Tb^{3+} and Tb^{3+}/Ho^{3+} doped phosphate glasses. *Opt. Mater.* **2008**, *30*, 1343–1348. [CrossRef]

26. Xia, S.; Guan, A.; Chen, P.; Wang, G.; Geng, Y.; Zhou, L. Sol-gel method for preparing a novel red-emitting phosphor $YVO_4:Sm^{3+},Eu^{3+}$ with ideal red color emission. *Superlattice* **2016**, *97*, 319–326. [CrossRef]

27. Blasse, G. *Luminescence Materials*; Springer: Berlin, Germany, 1994.

28. Blasse, G. *Materials Science of the Luminescence of Inorganic Solids*; Springer US: New York, NY, USA, 1978.

29. Dexter, D.L. A theory of sensitized luminescence in solids. *J. Chem. Phys.* **1953**, *21*, 836–850. [CrossRef]

30. Reisfeld, R.; Greenberg, E.; Velapoldi, R. Luminescence quantum efficiency of Gd and Tb in borate glasses and the mechanism of energy transfer between them. *J. Chem. Phys.* **1972**, *56*, 1698–1705. [CrossRef]